ACS APPLIED MATERIALS & INTERFACES

Research Article

www.acsami.org

Solution-Processed Planar Perovskite Solar Cell Without a Hole Transport Layer

Yi Jin and George Chumanov*

Department of Chemistry, Center for Optical Materials Science and Engineering Technologies (COMSET), Clemson University, Clemson, South Carolina 29634, United States

Supporting Information

ABSTRACT: Solar cells with a structure of ITO/ZnO/$CH_3NH_3PbI_3$/graphite/carbon black electrode were fabricated by spin coating at ambient conditions. PbI_2 thin films were converted into $CH_3NH_3PbI_3$ perovskite by reacting with CH_3NH_3I in solution. The incorporation of electrochemically exfoliated graphite improved the fill factor, open circuit potential and short circuit current density. The best device yielded 10.2% power conversion efficiency.

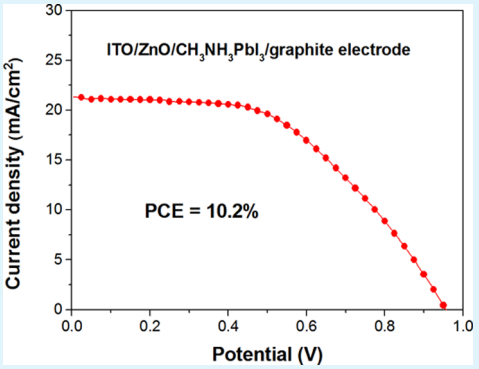

KEYWORDS: *solar cell, perovskite, zinc oxide, exfoliated graphite, solution-process*

INTRODUCTION

To achieve broad application of solar cells as a significant energy source, a balance between cost, stability and efficiency must be reached. Rapid evolution of lead halide perovskite solar cells, specifically by increasing power conversion efficiency, brought new potentials for their practical applications.[1−4] Lead halide perovskite materials were first used as dyes in liquid dye-sensitized solar cells in 2009.[4] A breakthrough in perovskite solar cells was achieved when the first solid-state mesoscopic heterojunction perovskite solar cell was built in 2012.[5,6] Planar heterojunction perovskite solar cells were further developed in 2013.[7,8] Power conversion efficiencies of mesoscopic heterojunction and planar heterojunction perovskite solar cells have exceeded 18%, while the most recent, verified perovskite solar cell efficiency is as high as 20.1%.[9−12] An important problem that needs to be addressed is how to decrease the manufacturing cost as well as improve the stability of the solar cells. Current perovskite solar cells often require high temperature processed TiO_2,[13] expensive fullerene derivatives,[9] or other unstable organic materials as electron/hole collecting layers,[11,14] and expensive rare metals (eg, silver or gold) as electrodes.[9,11] Also, the manufacturing process often requires high vacuum conditions and an oxygen free atmosphere. These factors add to the high manufacturing cost and thus hinder the widespread application of the solar cells.

Recent developments of carbon based perovskite solar cells have significantly reduced the manufacturing cost.[15−17] Carbon black and graphite have suitable work functions (about −5.0 eV) and can serve as a hole collecting electrode.[13,18] These solar cells often employ FTO/TiO_2 (dense layer)/TiO_2 or ZrO_2 (mesoporous layer)/$CH_3NH_3PbI_3$/carbon structures and require high temperature processing of TiO_2.[13,18] In contrast, ZnO compact layers can be easily prepared by spin coating ZnO nanoparticles at room temperature without heat treatment steps. Currently, ZnO based planar perovskite solar cells have achieved 15.7% efficiency.[19] The manufacturing cost can be further reduced by using ZnO as an *n*-type material in carbon based perovskite solar cells.

Another way to reduce the manufacturing cost is to optimize the solar cell structure. Perovskite solar cells utilize planar and mesoporous structures. Mesoporous structures are more favored because they prevent the direct contacts between cathodes and anodes. These structures also improve the electron injection, thereby minimizing the hysteresis effect.[20] In contrast, planar structures are simpler to manufacture because they do not need the additional mesoporous layer. Further simplification can be achieved by eliminating a dedicated hole transport layer. In this case, pinhole free perovskite films are required to avoid short circuits. It is well recognized that the quality of perovskite films plays an important role in achieving high efficiency solar cells in both planar and mesoscopic structures.[7,21−23]

In our previous work, a simple, reliable and scalable method for the fabrication of high quality $CH_3NH_3PbI_3$ thin films at room temperature based on the reaction of PbI_2 films with a saturated solution of CH_3NH_3I in 2-propanol/cyclohexane was

Received: March 10, 2015
Accepted: May 19, 2015
Published: May 19, 2015

DOI: 10.1021/acsami.5b02124
ACS Appl. Mater. Interfaces 2015, 7, 12015−12021

developed.[24] Here, this method, together with other solution processing methods were used to fabricate efficient planar perovskite solar cells. A planar ITO/ZnO/$CH_3NH_3PbI_3$/carbon electrode structure was selected to minimize the fabrication cost. These solar cells were built at ambient conditions at room temperature without a vacuum and inert atmosphere. This low cost method provides opportunities for the development of commercially viable perovskite solar cells.

EXPERIMENTAL SECTION

Materials. Fluorine doped tin oxide (FTO) glass (~7 Ω/sq) and indium tin oxide (ITO) glass (8−12 Ω/sq) were received from Sigma and Delta Technologies, LTD, respectively. Cyclohexane (Alfa Aesar, HPLC grade), 2-propanol (J. T. Baker, HPLC grade), *N*,*N*-dimethylformamide (DMF) (Sigma-Aldrich, 99.8%), sodium sulfate (Fisher Scientific, certified ACS grade), ammonium sulfate (Sigma-Aldrich, 99.0%), graphite rod (Alfa Aesar, 99%) and acetylene carbon black (50% compressed) (Strem Chemicals) were used as received. Methylammonium iodide, lead iodide and zinc oxide nanoparticles were synthesized following previously reported methods.[24]

Instrumentation. UV−vis extinction spectra were measured using a Shimadzu UV-2501 PC spectrophotometer. Electrochemical exfoliated graphite flakes were further dispersed in a VWR 750D ultrasonic cleaner. Powder X-ray diffraction (PXRD) data was collected using a Rigaku Ultima IV X-ray diffractometer with Cu Kα radiation (λ = 1.5418 Å) at 25 °C. Imaging and thickness measurements were performed using a AIST-NT SmartSPM-1000 atomic force microscopy (AFM) instrument operating in AC mode. Electron microscope images were obtained with an H-9500 transmission electron and an S-4800 field emission scanning electron microscopes (Hitachi). A Laurell WS-400B-6NPP-Lite Manual Spinner was used for spin-coating. PXRD pattern simulation was performed on Mercury 3.3 software by using a tetragonal $CH_3NH_3PbI_3$ single crystal structure (a = 8.849(2) Å, c = 12.642(2) Å and space group *I4cm*).[25] The current−voltage curves of solar cells were measured by using an electrochemical workstation (CH Instruments, CHI440) with linear sweep voltammetry. The solar cells were illuminated by an in-house built solar simulator equipped with a Mega-9 AM1.5G filter at a calibrated intensity of 100 mW cm^{-2}. The effective area of the solar cell was defined as 0.49 cm^2 with a nonreflective metal mask. The standard deviation was calculated from the measurements of eight solar cells. The impedance measurements were performed using Solartron analytical 1470E cell test system by applying a 0.015 V sinusoidal signal over the constant applied bias and the frequency range from 0.5 Hz to 100 kHz.

Electrochemical Exfoliation of Graphite. Mixtures of graphite particles and graphene sheets (from here on called graphite suspension) were obtained from electrochemically exfoliated (EE) graphite by a modified literature method.[26] Briefly, cathode and anode graphite rods were placed into Na_2SO_4 or $(NH_4)_2SO_4$ (0.50 mol L^{-1}, 800 mL) electrolyte solution at a distance of 2.0 cm. Electrochemical exfoliation was carried out at 5 °C by applying 10 V between the two graphite rods. After complete disintegration of the anode, the EE graphite was obtained in the form of a fluffy precipitate that was collected via vacuum filtration. The EE graphite was then washed three times with deionized water and two times with ethanol followed by dispersing in ethanol (30 mL). $NaBH_4$ (300 mg, 7.93 mmol) was added to the above suspension, and the reaction mixture was stirred at room temperature for 2 h. The EE graphite was collected by the vacuum filtration followed by washing three times with deionized water and two times with ethanol. A mixture of the EE graphite and 4-methyl-2-pentanone was sonicated at room temperature for 40 min. Following the centrifugation at 460*g* for 30 min to remove large particles, the supernatant containing ~0.8 mg mL^{-1} of graphite was used to fabricate all solar cells.

Solar Cell Fabrication. Devices were fabricated under an ambient environment. ITO coated glass substrates (1.5 cm × 2.5 cm) were masked by Scotch tape and etched by a mixture of 2.0 mol L^{-1} HCl and zinc powder. The substrates were then rinsed with 18 MΩ water followed by sonication in acetone, ethanol and water for 15 min in each solvent. The substrates were further cleaned by air plasma for 10 min. The substrates were coated with ZnO nanoparticles by spin-coating from $CHCl_3$/*n*-butanol suspension at 3000 rpm for 30 s. The spin coating was performed three times to obtain uniform films. Perovskite films were made according to previously described procedure.[24] PbI_2 (3.0 g) was dried in a vacuum oven at 120 °C for 20 min and dissolved in anhydrous DMF (6.0 mL) at 70 °C without stirring. It was found that stirring degraded the quality of the $CH_3NH_3PbI_3$ films by introducing pin holes, possibly from microscopic debris produced during the stirring process. After cooling to room temperature overnight, the PbI_2 solution was heated again at 70 °C for 2 h and then cooled to room temperature. After the second heating and cooling cycle, about 10 mg of insoluble precipitate was formed at the bottom of the container and further removed and discarded. The supernatant solution was used for spin coating. The purification process of PbI_2 solution reduced the formation of pin holes in $CH_3NH_3PbI_3$ films. 100 μL of PbI_2 solution was dropped onto glass/ITO/ZnO substrates multiple times until the solution completely covered the surface. After waiting 2 min, the substrates were spun at 3000 rpm for 3 min under a continuous flow of clean air. After drying in air, the substrates were immersed for 5 h into CH_3NH_3I saturated solution in 5/95 (v/v) 2-propanol/cyclohexane. The graphite layer was fabricated by spin coating of the graphite suspension in 4-methyl-2-pentanone. 100 μL of the suspension was delivered drop by drop at the rate of one drop per 15 s onto a substrate spinning at 1000 rpm. To make the direct electrical contact to the ITO substrate, all layers were removed from a small area by wiping with cotton swabs wetted in acetone and, separately, 2 M HCl aqueous solution. Acetylene carbon black was used to improve electrical contact between graphite layer and the top electrode that was either FTO coated glass, copper or any other metal. For convenience purposes, flat FTO coated glass was mainly used as the top electrode for the devices reported here. The entire structure was mechanically clamped together with two binder clips.

RESULTS AND DISCUSSION

Electrochemical exfoliation is an effective method for disintegrating bulk graphite. The resultant EE graphite can be dispersed in appropriate solvents to produce a suspension containing a mixture of graphite particles and graphene sheets.[26] Graphene sheets prepared by this method were shown to exhibit hole mobility of ~310 cm^2 V^{-1} S^{-1}.[26] The high hole mobility supports the efficient hole extraction from semiconductors, thereby increasing the power conversion efficiency in solar cells. The electrochemical exfoliation of graphite rods was performed in a two electrode system in Na_2SO_4 and $(NH_4)_2SO_4$ electrolytes. It was found that the concentration of Na_2SO_4 affected the yield of EE graphite. After various concentrations (0.10, 0.25, 0.50, 0.75 and 1.0 mol L^{-1}) were tested, 0.5 mol L^{-1} was found to be optimal and was used throughout the studies. The same concentration of $(NH_4)_2SO_4$ consistently yielded 4−5 times less graphite particles and graphene sheets. The exfoliation at lower temperature produced graphite suspensions with higher concentrations of graphite particles and graphene sheets. Several solvents such as dimethylformamide (DMF), acetone, ethyl acetate, chlorobenzene, 1,2-dichlorobenzene, 2,4-dimethyl-3-pentanone, cyclopentanone and 4-methyl-2-pentanone were tested to optimize the graphite suspension. The EE graphite was dispersed in each solvent by sonicating for 15 min at room temperature followed by centrifuging at 460*g*. Only DMF and 4-methyl-2-pentanone produced stable graphite suspensions after the centrifugation, whereas the other solvents gave a clear supernatant and a black precipitate. Even though the DMF suspensions contained higher concentrations of graphite particles and graphene sheets,

DOI: 10.1021/acsami.5b02124
ACS Appl. Mater. Interfaces 2015, 7, 12015−12021

4-methyl-2-pentanone graphite suspensions were used in the device fabrication, because DMF dissolved $CH_3NH_3PbI_3$.

When this suspension was spin-coated onto $CH_3NH_3PbI_3$ films and heated at 60 °C for 5 min, the color of the films changed from deep brown to yellow. The graphite was not expected to interact with $CH_3NH_3PbI_3$, therefore the color change was ascribed to the oxidation of I^- to I_2 by oxidizing groups that were present on the surface of the graphite and produced during the anodic exfoliation of graphite rods. The oxidation reaction was confirmed in an independent experiment, in which NaI solution exposed to EE graphite in 4-methyl-2-pentanone produced a strong absorption peak at 358 nm due to I_3^-.[27]

The stability of $CH_3NH_3PbI_3$ films was significantly improved after the EE graphite was treated with $NaBH_4$ prior to dispersing in 4-methyl-2-pentanone. The films remained brown after heating for 15 min at 100 °C. $SnCl_2$ was also tested as a possible reductant for EE graphite, but this treatment rendered graphite indispersible in 4-methyl-2-pentanone. To characterize the morphology of the graphite after the treatment with $NaBH_4$, the suspension was drop-casted on a silicon wafer and imaged with AFM. As can be seen in Figure 1, the majority

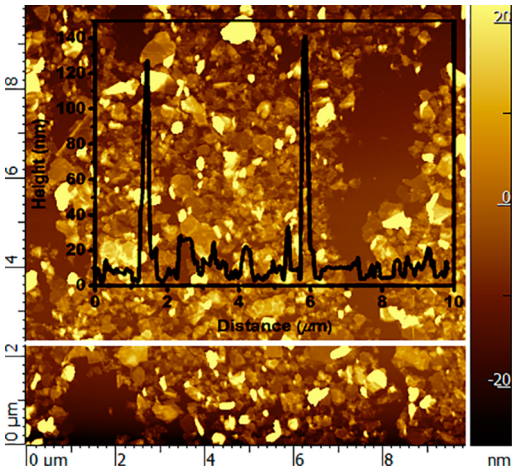

Figure 1. AFM image of graphite treated with $NaBH_4$ and drop-casted on a silicon wafer from 4-methyl-2-pentanone suspension. Inset: height profile along the white line.

of graphite was in the form of nanoparticles with a small amount of two-dimensional graphene sheets. The thickness of the majority graphene sheets was measured to be less than 10 nm with less than 30 atomic layers in the sheet. This morphology was quite different from that previously reported in similar exfoliation experiments, in which the yield of graphene (≤3 layers) in excess of 85% was observed.[26] The apparent discrepancy could be from the fact that graphite rods were used in this study instead of graphite sheets used in the referenced work.

The devices were fabricated by the sequential deposition of ZnO, perovskite, graphite and carbon black layers on ITO substrates, as described in Experimental Section. The thickness of ZnO and $CH_3NH_3PbI_3$ layers was previously optimized,[19] and no further optimization was required in this study. The formation of the perovskite films was confirmed by XRD (Figure 2a).[6] AFM and SEM images revealed compacted and uniform films with 21 nm RMS roughness (Figure 2b and Figure S2a of the Supporting Information). The band-edge absorption for $CH_3NH_3PbI_3$ was observed at 783 nm (Figure 2c). The total absorption of the glass/ITO/ZnO/$CH_3NH_3PbI_3$/graphite structure increased after spin-coating a graphite layer and reached the instrument saturation level at wavelengths shorter than 475 nm (Figure 2c). The graphite layer completely covered the surface of the $CH_3NH_3PbI_3$, as was confirmed by AFM and SEM (Figure 2d and Figure S3a of the Supporting Information).

Both forward and reversed scans of ITO/ZnO/$CH_3NH_3PbI_3$/carbon black/FTO solar cell (without graphite layer) produced a short circuit current density (J_{sc}) more than 15 mA cm^{-2} but a low fill factor (FF) (Figure 3). The open circuit potential (V_{oc}) in the reverse and forward scans was measured to be 0.91 and 0.80 V, respectively, indicating a strong hysteresis effect previously also observed for planar perovskite solar cells.[28,29] Even though the mechanism of the hysteresis effect is not completely understood, it is often ascribed to the deficient extraction of carriers leading to complex charging/discharging phenomena as well as the residual polarization associated with structural changes in the perovskite material.[20,28−33] Wojciechowski et al. have minimized the hysteresis effect by improving the electron injection into TiO_2 at the interface with $CH_3NH_3PbI_{3-x}Cl_x$.[29] In our case, the hysteresis could be due to the phenomena at both ZnO/$CH_3NH_3PbI_3$ and $CH_3NH_3PbI_3$/ (graphite) carbon black interfaces; however, improving FF and the efficiency is more important for the operation of the cell. Good efficiencies and FF were previously demonstrated in perovskite solar cells with ZnO as an electron extraction layer,[19] Therefore, the low efficiency and FF observed for ITO/ZnO/$CH_3NH_3PbI_3$/carbon black/FTO solar cell was ascribed to be due to the interface between $CH_3NH_3PbI_3$ and carbon black.

The optimization of the interface was made by inserting a layer of graphite between $CH_3NH_3PbI_3$ and the carbon black electrode. In method B (Table 1), the thickness of the graphite layer was increased relative to that in method A by spin-coating twice the amount of the graphite suspension. No significant improvement was observed of the cell characteristics including the power conversion efficiency (PCE), indicating that the charge collection efficiency of the thinner graphite layer was already at its maximum. In method C, the graphite layer was first deposited onto a PbI_2 film followed by converting lead iodide into perovskite to give an *in situ* converted device. It was previously reported that the efficiency of perovskite solar cells significantly increased when candle soot was deposited on PbI_2 prior to converting into perovskite.[18] The characteristics of our *in situ* converted devices did not change significantly except of the apparent decrease of the hysteresis. V_{oc}, J_{sc} and FF for the reverse and forward scans were consistently closer to each other. In method D, the graphite suspension prepared by the electrochemical exfoliation in $(NH_4)_2SO_4$ electrolyte was used. Not only the $(NH_4)_2SO_4$ electrolyte produced lower yields of the graphite suspension, the performance of the devices was slightly inferior to that of devices made with Na_2SO_4 graphite suspensions. The stability of the devices made by method A was examined by storing them at the ambient atmosphere and in a desiccator at room temperature for two months. The devices stored at the ambient atmosphere exhibited yellowing and the significant performance degradation. Storing in the desiccator resulted in a slight decrease of the average PCE from 7.3 ± 0.8% to 6.7 ± 0.6% as measured in the reverse scan at 0.01 V s^{-1}. These results indicate that the structure is inherently stable providing that moisture is eliminated. Additional packaging and

DOI: 10.1021/acsami.5b02124
ACS Appl. Mater. Interfaces 2015, 7, 12015−12021

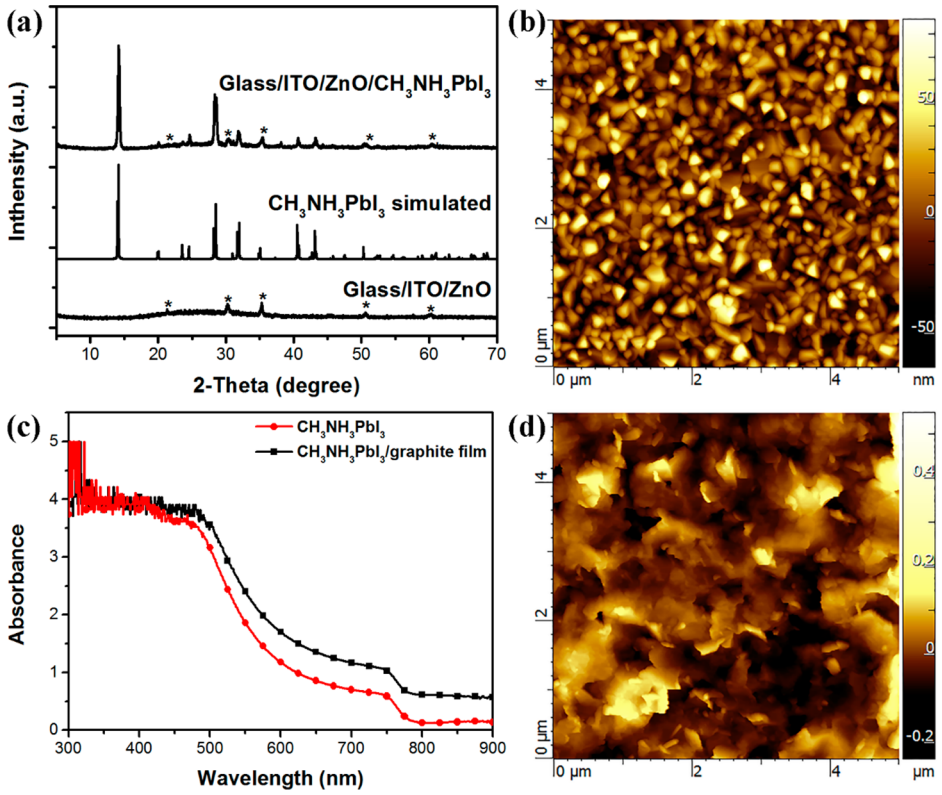

Figure 2. (a) XRD spectrum of a $CH_3NH_3PbI_3$ film on glass/ITO/ZnO substrate, XRD spectrum of the glass/ITO/ZnO substrate and simulated XRD spectrum of tetragonal $CH_3NH_3PbI_3$. Diffraction peaks at 14.02°, 19.97°, 24.55°, 28.52°, 31.68°, 40.51° and 43.11° were assigned as the (110), (020), (022), (220), (222), (040) and (330) planes of tetragonal perovskite, respectively. (b) AFM image of a $CH_3NH_3PbI_3$ film on glass/ITO/ZnO substrate (c) UV−vis spectra of $CH_3NH_3PbI_3$ and $CH_3NH_3PbI_3$/graphite films on glass/ITO/ZnO substrates. (d) AFM image of the graphite film on a glass/ITO/ZnO/$CH_3NH_3PbI_3$ substrate.

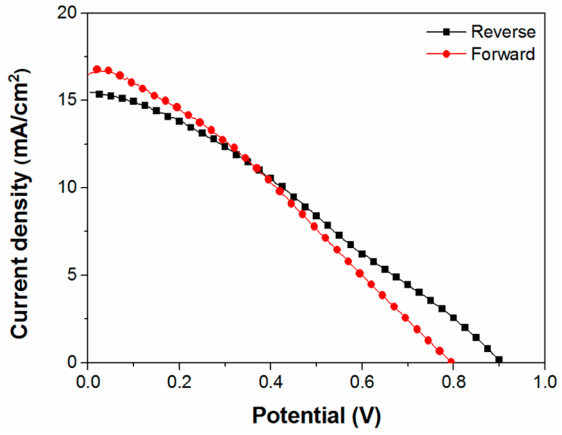

Figure 3. $J-V$ curves of a glass/ITO/ZnO/$CH_3NH_3PbI_3$/carbon black/FTO solar cell measured at 0.01 V s^{-1} scan rate. Forward scan was from 0.0 to 1.0 V and the reverse scan was from 1.0 to 0.0 V.

sealing the devices is required when solar applications are considered.

$J-V$ curves of solar cells are commonly measured by applying a compensating potential that is scanned from zero to a potential slightly larger than V_{oc}. The scan direction of the compensating potential has a noticeable effect on the performance of the devices reported here, but the effect was smaller from that previously reported for the similar structures.[20,28−33] The hysteresis was studied as a function of the scan rate and scan direction, revealing different hysteresis for different structures (Figure 4 and Table 2). The apparent performance of a device improved and the hysteresis decreased as the scan rate increased. The short circuit current, J_{sc}, also increased with the scan rate, especially in the reverse scan. The best device fabricated in this work showed increased V_{oc} to 0.960 V in the reverse scan from 0.915 V in the forward scan. Also, reverse scans always yielded higher fill factors. On the basis of these results, it seems more appropriate to report device characteristics as measured in the reverse scan with a slow scan rate starting from a potential close to V_{oc} because the system is expected to be more in equilibrium.

Electrochemical impedance spectroscopy (EIS) can potentially provide insights into charge transfer processes across interfaces in solar cells. EIS data is often fit into an equivalent electrical circuit, and great effort is made to assign each element in the circuit to a specific charge transfer process in the device. Here, we took a different approach, in which EIS spectra from two different structures, specifically devices with and without graphite layer, are compared to each other using Nyquist plots (Figure 5). Such relative comparison allowed us to focus only on perovskite/graphite electrical contact that was determined to have the largest effect on the overall performance of the studied devices. The spectra were acquired at 0 and 0.550 V forward potential bias from 0.5 Hz to 100 kHz with 0.015 V potential modulation. The latter bias was selected because it was in the same region where all tested devices produced the maximum power. The devices without the graphite layer (carbon black was directly deposited onto the perovskile layer) exhibited two characteristic semicircle-like features. The radius of the first, high frequency circle corresponded to the electron

DOI: 10.1021/acsami.5b02124
ACS Appl. Mater. Interfaces 2015, 7, 12015−12021

Table 1. Device Characteristics for Solar Cells Prepared with Different Deposition Methods of the Graphite Layer[a]

method	scan direction	V_{oc} (V)	J_{sc} (mA cm^{-2})	FF	PCE (%)
A	reverse	0.94 ± 0.02	12.9 ± 2.0	0.61 ± 0.11	7.3 ± 0.8
	forward	0.86 ± 0.02	20.1 ± 0.7	0.38 ± 0.04	6.7 ± 0.9
B	reverse	0.95 ± 0.01	14.1 ± 1.4	0.54 ± 0.06	7.2 ± 0.3
	forward	0.84 ± 0.01	21.4 ± 0.8	0.37 ± 0.01	6.6 ± 0.3
C	reverse	0.91 ± 0.04	12.3 ± 2.1	0.58 ± 0.05	6.4 ± 0.8
	forward	0.88 ± 0.02	15.2 ± 2.4	0.45 ± 0.03	6.0 ± 0.9
D	reverse	0.92 ± 0.01	11.6 ± 0.7	0.54 ± 0.02	5.8 ± 0.6
	forward	0.88 ± 0.01	17.9 ± 1.1	0.37 ± 0.01	5.8 ± 0.6

[a]Solar cell structure ITO/ZnO/$CH_3NH_3PbI_3$/graphite/carbon black electrode. Na_2SO_4 was used as the electrolyte to exfoliate graphite in methods A, B and C; $(NH_4)_2SO_4$ was used as the electrolyte in D. 100 μL of graphite suspension was spin-coated on the $CH_3NH_3PbI_3$ film in A and D; 200 μL of the suspension was used in B. In C, 100 μL of graphite suspension was spin-coated on a PbI_2 film followed by converting to $CH_3NH_3PbI_3$. Device characteristics were measured at scan rate of 0.01 V s^{-1}. Forward scan was from 0.0 to 1.0 V, reverse scan was from 1.0 to 0.0 V.

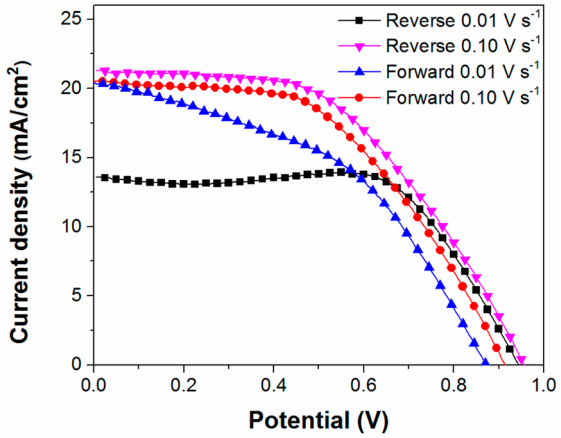

Figure 4. $J-V$ curves of planar perovskite solar cell, ITO/ZnO/$CH_3NH_3PbI_3$/graphite/carbon black electrode, measured at scan rates 0.01 and 0.10 V s^{-1}. Forward scan was from 0.0 to 1.0 V, reverse scan was from 1.0 to 0.0 V.

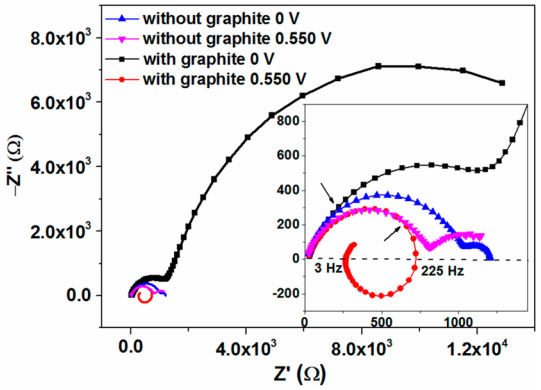

Figure 5. Nyquist plots of perovskite solar cells made with (method A) and without a graphite layer as measured in dark at 0 and 0.550 V forward bias. Inset: zoom in of the low impedance region. Arrows indicate points, at which the corresponding curves start to deviate from each other.

Table 2. Best Device Performance under Different Scan Conditions[a]

scan rate (V s^{-1})	scan direction	V_{oc} (V)	J_{sc} (mA cm^{-2})	FF	PCE (%)
0.01	reverse	0.945	13.6	0.67	8.6
0.10	reverse	0.960	21.3	0.50	10.2
0.01	forward	0.875	20.4	0.45	8.1
0.10	forward	0.915	20.5	0.50	9.4

[a]Forward scan was from 0.0 to 1.0 V, reverse scan was from 1.0 to 0.0 V.

transfer resistance through ITO/ZnO/perovskite and carbon black/back electrode (Figure 5). This assignment was made based on largely unaltered Nyquist plots for all devices in this frequency region as well as the fact that these layers were the same for all devices. The electron transfer exhibited both capacitive and resistive characters due to the polarization of the corresponding interfaces and the finite electron transfer rates through the interfaces and materials. The similar assignments were previously made for other solar cells.[34,35] As expected, the overall electron transfer resistance dropped at 0.550 V bias relative to that at zero bias for devices without the graphite layer (Figure 5).

When the graphite layer was incorporated into devices, dramatic changes in the Nyquist plots were observed in the low frequency region. The overall electron transfer resistance increased by more than an order of magnitude at zero bias but dropped back to the previous values when 0.550 V bias was applied. The increase of the resistance was likely due to the initial formation of a poor electrical contact between the perovskite and graphite layers. This contact was substantially improved when the bias was applied. It is well-known that electrical contacts could exhibit large resistance at low applied potential differences but became highly conductive when the potential difference is increased. Besides, the resistance at zero bias is not important for the device operation because these devices are intended to operate under internal bias around 0.550 V.

A region of the negative capacitance can also be seen in the Nyquist plot at 0.550 V bias in the frequency range between 3 and 225 Hz (Figure 5). The region of the negative capacitance implies the inductive-like behavior characterized by the current lagging the applied potential. There is no firm consensus among explanations of the negative capacitance observed in solar cells. The ionic conductivity is often involved for the explanation;[34] it is also known that Schottky and $p-n$-junctions can exhibit inductive-like behavior.[34,36,37] A common factor in these cases is the presence of nonohmic (nonlinear) conductivity. The incorporation of graphite between the perovskite and carbon black layers created two interfaces: graphite/carbon black and perovskite/graphite. Both interfaces acted as resistors and, when a bias was applied, the current produced a potential drop and polarization across each interface. Whereas the first interface is expected to behave as a liner resistor, the second one could exhibit a nonlinear

DOI: 10.1021/acsami.5b02124
ACS Appl. Mater. Interfaces 2015, 7, 12015−12021

resistance: the resistance becomes a function of the passing current.[36] This nonlinear resistance could result from ions in perovskite moving in and out the interfacial region when the polarization changed.[38] It is expected that, when AC potential is applied to such system, the current will lag the applied potential leading to the inductive-like response and the negative capacitance. It was previously shown that ions can move in the perovskite under applied bias.[38] The fact that the negative capacitance was seen at low frequencies indicated a slow process that could be associated with the ionic conductivity in the perovskite.

CONCLUSION

A simple, potentially low cost method based on benchtop wet chemistry for fabricating efficient perovskite solar cells with a structure of ITO/ZnO/$CH_3NH_3PbI_3$/graphite/carbon black electrode is described. All films were deposited by spin coating under ambient conditions without heat treatment. The structures did not have a designated hole-transport layer; instead an electrochemically exfoliated graphite layer increased the power conversion efficiency by improving the electrical contact between perovskite and the hole collecting electrode. The best device demonstrated a PCE of 10.2%, V_{oc} of 0.960 V and J_{sc} of 21.3 mA cm^{-2} as measured at a 0.10 V s^{-1} scan rate. The reported method presents more opportunities for achieving a low cost perovskite solar cell.

ASSOCIATED CONTENT

Supporting Information

Syntheses of ZnO nanoparticles, TEM image of ZnO nanoparticles, SEM and AFM images of ZnO film on a glass/ITO substrate, UV−vis spectrum of ZnO film on a quartz substrate, SEM, AFM images and UV−vis spectrum of $CH_3NH_3PbI_3$ on a glass/ITO/ZnO substrate, SEM and AFM images of graphite layer on a glass/ITO/ZnO/$CH_3NH_3PbI_3$ substrate, UV−vis spectrum of graphite films on quartz and glass/ITO/ZnO/$CH_3NH_3PbI_3$ substrates, and PCE distribution for devices. The Supporting Information is available free of charge on the ACS Publications website at DOI: 10.1021/acsami.5b02124.

AUTHOR INFORMATION

Corresponding Author

*G. Chumanov. E-mail: gchumak@clemson.edu.

Notes

The authors declare no competing financial interest.

ACKNOWLEDGMENTS

We gratefully acknowledge the support of this work through Department of Energy, Grant DE-FG02-06ER46342, and Clemson University Center for Optical Materials Science and Engineering Technologies. Special thanks to Stephen E. Creager, Jamie A. Shetzline and Lakshman K. Ventrapragada for the help with EIS measurements.

REFERENCES

(1) Kazim, S.; Nazeeruddin, M. K.; Graetzel, M.; Ahmad, S. Perovskite as Light Harvester: A Game Changer in Photovoltaics. *Angew. Chem., Int. Ed.* **2014**, *53*, 2812−2824.

(2) Snaith, H. J. Perovskites: The Emergence of a New Era for Low-Cost, High-Efficiency Solar Cells. *J. Phys. Chem. Lett.* **2013**, *4*, 3623−3630.

(3) Hodes, G. Perovskite-based Solar Cells. *Science* **2013**, *342*, 317−318.

(4) Kojima, A.; Teshima, K.; Shirai, Y.; Miyasaka, T. Organometal Halide Perovskites as Visible-Light Sensitizers for Photovoltaic Cells. *J. Am. Chem. Soc.* **2009**, *131*, 6050−6051.

(5) Kim, H.-S.; Lee, C.-R.; Im, J.-H.; Lee, K.-B.; Moehl, T.; Marchioro, A.; Moon, S.-J.; Humphry-Baker, R.; Yum, J.-H.; Moser, J. E.; Graetzel, M.; Park, N.-G. Lead Iodide Perovskite Sensitized All-Solid-State Submicron Thin Film Mesoscopic Solar Cell with Efficiency Exceeding 9%. *Sci. Rep.* **2012**, *2*, 591.

(6) Lee, M. M.; Teuscher, J.; Miyasaka, T.; Murakami, T. N.; Snaith, H. J. Efficient Hybrid Solar Cells Based on meso-Superstructured Organometal Halide Perovskites. *Science* **2012**, *338*, 643−647.

(7) Liu, M. Z.; Johnston, M. B.; Snaith, H. J. Efficient Planar Heterojunction Perovskite Solar Cells by Vapour Deposition. *Nature* **2013**, *501*, 395−398.

(8) Jeng, J.-Y.; Chiang, Y.-F.; Lee, M.-H.; Peng, S.-R.; Guo, T.-F.; Chen, P.; Wen, T.-C. $CH_3NH_3PbI_3$ Perovskite/Fullerene Planar-Heterojunction Hybrid Solar Cells. *Adv. Mater.* **2013**, *25*, 3727−3732.

(9) Nie, W.; Gupta, G.; Mohite, A. D.; Tsai, H.; Blancon, J.-C.; Crochet, J. J.; Wang, H.-L.; Asadpour, R.; Alam, M. A.; Neukirch, A. J.; Chhowalla, M.; Tretiak, S. High-Efficiency Solution-Processed Perovskite Solar Cells with Millimeter-Scale Grains. *Science* **2015**, *347*, 522−525.

(10) Jeon, N. J.; Noh, J. H.; Yang, W. S.; Kim, Y. C.; Ryu, S.; Seo, J.; Seok, S. I. Compositional Engineering of Perovskite Materials for High-Performance Solar Cells. *Nature* **2015**, *517*, 476−480.

(11) Zhou, H.; Chen, Q.; Li, G.; Luo, S.; Song, T.-b.; Duan, H.-S.; Hong, Z.; You, J.; Liu, Y.; Yang, Y. Interface Engineering of Highly Efficient Perovskite Solar Cells. *Science* **2014**, *345*, 542−546.

(12) Kamat, P. V. Emergence of New Materials for Light−Energy Conversion: Perovskites, Metal Clusters, and 2-D Hybrids. *J. Phys. Chem. Lett.* **2014**, *5*, 4167−4168.

(13) Mei, A.; Li, X.; Liu, L.; Ku, Z.; Liu, T.; Rong, Y.; Xu, M.; Hu, M.; Chen, J.; Yang, Y.; Han, H.; Gratzel, M. A Hole-Conductor-Free, Fully Printable Mesoscopic Perovskite Solar Cell with High Stability. *Science* **2014**, *345*, 295−298.

(14) Wang, W.; Yuan, J.; Shi, G.; Zhu, X.; Shi, S.; Liu, Z.; Han, L.; Wang, H.-Q.; Ma, W. Inverted Planar Heterojunction Perovskite Solar Cells Employing Polymer as the Electron Conductor. *ACS Appl. Mater. Interfaces* **2015**, *7*, 3994−3999.

(15) Wei, Z.; Chen, H.; Yan, K.; Yang, S. Inkjet Printing and Instant Chemical Transformation of a $CH_3NH_3PbI_3$/Nanocarbon Electrode and Interface for Planar Perovskite Solar Cells. *Angew. Chem.* **2014**, *126*, 13455−13459.

(16) Yan, K.; Wei, Z.; Li, J.; Chen, H.; Yi, Y.; Zheng, X.; Long, X.; Wang, Z.; Wang, J.; Xu, J.; Yang, S. High-Performance Graphene-based Hole Conductor-Free Perovskite Solar Cells: Schottky Junction Enhanced Hole Extraction and Electron Blocking. *Small* **2015**, *11*, 2269−2274.

(17) Chen, H.; Wei, Z.; Yan, K.; Yi, Y.; Wang, J.; Yang, S. Liquid Phase Deposition of TiO_2 Nanolayer Affords $CH_3NH_3PbI_3$/Nanocarbon Solar Cells with High Open-Circuit Voltage. *Faraday Discuss.* **2015**, *176*, 271−286.

(18) Wei, Z.; Yan, K.; Chen, H.; Yi, Y.; Zhang, T.; Long, X.; Li, J.; Zhang, L.; Wang, J.; Yang, S. Cost-Efficient Clamping Solar Cells Using Candle Soot for Hole Extraction from Ambipolar Perovskites. *Energy Environ. Sci.* **2014**, *7*, 3326−3333.

(19) Liu, D.; Kelly, T. L. Perovskite Solar Cells with a Planar Heterojunction Structure Prepared Using Room-Temperature Solution Processing Techniques. *Nat. Photonics* **2014**, *8*, 133−138.

(20) Unger, E. L.; Hoke, E. T.; Bailie, C. D.; Nguyen, W. H.; Bowring, A. R.; Heumuller, T.; Christoforo, M. G.; McGehee, M. D. Hysteresis and Transient Behavior in Current-Voltage Measurements of Hybrid-Perovskite Absorber Solar Cells. *Energy Environ. Sci.* **2014**, *7*, 3690−3698.

(21) Eperon, G. E.; Burlakov, V. M.; Docampo, P.; Goriely, A.; Snaith, H. J. Morphological Control for High Performance, Solution-

DOI: 10.1021/acsami.5b02124
ACS Appl. Mater. Interfaces 2015, 7, 12015−12021

Processed Planar Heterojunction Perovskite Solar Cells. *Adv. Funct. Mater.* **2014**, *24*, 151−157.
(22) Chen, Q.; Zhou, H.; Hong, Z.; Luo, S.; Duan, H.-S.; Wang, H.-H.; Liu, Y.; Li, G.; Yang, Y. Planar Heterojunction Perovskite Solar Cells via Vapor-Assisted Solution Process. *J. Am. Chem. Soc.* **2014**, *136*, 622−625.
(23) Zhang, W.; Saliba, M.; Pathak, S. K.; Horantner, M. T.; Stergiopoulos, T.; Stranks, S. D.; Eperon, G. E.; Alexander-Webber, J. A.; Abate, A.; Chen, Y.; Snaith, H. J.; Moore, D. T.; Wiesner, U.; Sadhanala, A.; Friend, R. H.; Yao, S.; Estroff, L. A. Ultrasmooth Organic-Inorganic Perovskite Thin-Film Formation and Crystallization for Efficient Planar Heterojunction Solar Cells. *Nat. Commun.* **2015**, *6*, 6142.
(24) Jin, Y.; Chumanov, G. Fabrication of Lead Halide Perovskite Film by Controlling Reactivity at Room Temperature in Mixed Solvents. *Chem. Lett.* **2014**, *43*, 1722−1724.
(25) Stoumpos, C. C.; Malliakas, C. D.; Kanatzidis, M. G. Semiconducting Tin and Lead Iodide Perovskites with Organic Cations: Phase Transitions, High Mobilities, and near-Infrared Photoluminescent Properties. *Inorg. Chem.* **2013**, *52*, 9019−9038.
(26) Parvez, K.; Wu, Z.-S.; Li, R.; Liu, X.; Graf, R.; Feng, X.; Muellen, K. Exfoliation of Graphite into Graphene in Aqueous Solutions of Inorganic Salts. *J. Am. Chem. Soc.* **2014**, *136*, 6083−6091.
(27) Awtrey, A. D.; Connick, R. E. The Absorption Spectra of I^2, I^{3-}, I^-, IO^{3-}, $S_4O_6^=$ and $S_2O_3^=$. Heat of the Reaction $I^{3-} = I_2 + I^-$. *J. Am. Chem. Soc.* **1951**, *73*, 1842−1843.
(28) Shao, Y.; Xiao, Z.; Bi, C.; Yuan, Y.; Huang, J. Origin and Elimination of Photocurrent Hysteresis by Fullerene Passivation in $CH_3NH_3PbI_3$ Planar Heterojunction Solar Cells. *Nat. Commun.* **2014**, *5*, 5784.
(29) Wojciechowski, K.; Stranks, S. D.; Abate, A.; Sadoughi, G.; Sadhanala, A.; Kopidakis, N.; Rumbles, G.; Li, C.-Z.; Friend, R. H.; Jen, A. K. Y.; Snaith, H. J. Heterojunction Modification for Highly Efficient Organic-Inorganic Perovskite Solar Cells. *ACS Nano* **2014**, *8*, 12701−12709.
(30) Tress, W.; Marinova, N.; Moehl, T.; Zakeeruddin, S. M.; Nazeeruddin, M. K.; Gratzel, M. Understanding the Rate-Dependent J-V Hysteresis, Slow Time Component, and Aging in $CH_3NH_3PbI_3$ Perovskite Solar Cells: The Role of a Compensated Electric Field. *Energy Environ. Sci.* **2015**, *8*, 995−1004.
(31) Chen, H.-W.; Sakai, N.; Ikegami, M.; Miyasaka, T. Emergence of Hysteresis and Transient Ferroelectric Response in Organo-Lead Halide Perovskite Solar Cells. *J. Phys. Chem. Lett.* **2015**, *6*, 164−169.
(32) Kim, H.-S.; Park, N.-G. Parameters Affecting I-V Hysteresis of $CH_3NH_3PbI_3$ Perovskite Solar Cells: Effects of Perovskite Crystal Size and Mesoporous TiO_2 Layer. *J. Phys. Chem. Lett.* **2014**, *5*, 2927−2934.
(33) Sanchez, R. S.; Gonzalez-Pedro, V.; Lee, J.-W.; Park, N.-G.; Kang, Y. S.; Mora-Sero, I.; Bisquert, J. Slow Dynamic Processes in Lead Halide Perovskite Solar Cells. Characteristic Times and Hysteresis. *J. Phys. Chem. Lett.* **2014**, *5*, 2357−2363.
(34) Dualeh, A.; Moehl, T.; Tetreault, N.; Teuscher, J.; Gao, P.; Nazeeruddin, M. K.; Gratzel, M. Impedance Spectroscopic Analysis of Lead Iodide Perovskite-Sensitized Solid-State Solar Cells. *ACS Nano* **2014**, *8*, 362−373.
(35) Conings, B.; Baeten, L.; Boyen, H.-G.; Spoltore, D.; D'Haen, J.; Grieten, L.; Wagner, P.; Van Bael, M. K.; Manca, J. V. Influence of Interface Morphology onto the Photovoltaic Properties of Nano-patterned ZnO/Poly(3-hexylthiophene) Hybrid Solar Cells. An Impedance Spectroscopy Study. *J. Phys. Chem. C* **2011**, *115*, 16695−16700.
(36) Bisquert, J. A Variable Series Resistance Mechanism to Explain the Negative Capacitance Observed in Impedance Spectroscopy Measurements of Nanostructured Solar Cells. *Phys. Chem. Chem. Phys.* **2011**, *13*, 4679−4685.
(37) van den Biesen, J. J. H. Modelling the Inductive Behaviour of Short-Base p-n Junction Diodes at High Forward Bias. *Solid-State Electron.* **1990**, *33*, 1471−1476.
(38) Zhang, Y.; Liu, M.; Eperon, G. E.; Leijtens, T.; McMeekin, D. P.; Saliba, M.; Zhang, W.; De Bastiani, M.; Petrozza, A.; Herz, L.; Johnston, M. B.; Lin, H.; Snaith, H. Charge Selective Contacts, Mobile Ions and Anomalous Hysteresis in Organic-inorganic Perovskite Solar Cells. *Mater. Horiz.* **2015**, *2*, 315−322.

DOI: 10.1021/acsami.5b02124
ACS Appl. Mater. Interfaces 2015, 7, 12015−12021